Journal of Alloys and Compounds 509 (2011) 3074–3079

Contents lists available at ScienceDirect

Journal of Alloys and Compounds

journal homepage: www.elsevier.com/locate/jallcom

Nanocrystalline $Fe_{1-x}Co_xSn_2$ solid solutions prepared by reduction of salts in tetraethylene glycol

Uche G. Nwokeke[a], Alan V. Chadwick[b], Ricardo Alcántara[a], Maria Alfredsson[b], José L. Tirado[a,*]

[a] Laboratorio de Química Inorgánica, Universidad de Córdoba, Edificio C3, Campus de Rabanales, 14071 Córdoba, Spain
[b] Functional Materials Group, School of Physical Sciences, University of Kent, Canterbury, Kent CT2 7NH, UK

ARTICLE INFO

Article history:
Received 23 September 2010
Received in revised form
27 November 2010
Accepted 30 November 2010
Available online 7 December 2010

Keywords:
Cobalt tin intermetallic compound
Iron tin intermetallic compound
Lithium batteries anode
Mössbauer spectroscopy

ABSTRACT

In an effort to improve the electrochemical performance of tin intermetallic phases as electrode active material for lithium-ion batteries, $Fe_{1-x}Co_xSn_2$ solid solutions with $x = 0.0$, 0.25, 0.3, 0.5, 0.6 and 0.8 were prepared by chemical reduction in tetraethylene glycol. Precise control of the synthesis conditions allowed single-phase nanocrystalline materials to be prepared, with particle diameters of about 20 nm and cubic, nanorods, and U-shaped morphologies. The substitution of iron by cobalt induced a contraction of the unit cell volume. The hyperfine parameters of the ^{57}Fe Mössbauer spectra were sensitive to the Co/Fe substitution and revealed a superparamagnetic behaviour. In lithium cells nanocrystalline $Fe_{1-x}Co_xSn_2$ active materials delivered reversible capacities above 500 mAh g^{-1} that depended on the composition and cycling conditions. The intermediate compositions exhibit better electrochemical performance than the end compositions $CoSn_2$ and $FeSn_2$.

1. Introduction

Intermetallic compounds containing tin atoms are excellent electrode active materials for lithium ion batteries. The alloys that contain cobalt are particularly promising because they show great ability to form nanostructured particles and exhibit excellent stability and capacity retention [1]. Thus, several studies on CoSn [2], $CoSn_2$ [3,4], and Co_3Sn_2 [4] have been reported. Also carbon [5,6] and polymer [7,8] additives were recently found useful to improve the performance. Pure $CoSn_3$ is difficult to prepare at high temperature [9]. Microcrystalline CoSn [2] and Co_3Sn_2 [4,10,11] show very little ability to react with lithium, but in the amorphous state or with very small particle size, these solids can exhibit high capacities. Microcrystalline $CoSn_2$ was studied by Ionica-Bousquet et al. [3] and a high reactivity with lithium was observed. Recently, nano-sized Co–Sn alloy anodes were studied in lithium cells, and a two-step electrochemical reaction mechanism of $CoSn_2$ alloy with Li^+ was confirmed [12].

Due to cost and toxicity factors, the substitution of cobalt by iron in successful cobalt–tin intermetallics would be advantageous. Similarly, by using only a partial substitution, the best properties of $CoSn_x$ phases might be preserved. The intermetallic compounds $FeSn_2$ and $CoSn_2$ are isostructural (space group *I*4/*mcm*). The former was first studied by Mao et al. [13], and it was found that the reaction of lithium with Sn–Fe alloys leads to Li–Sn alloys and nanometer-sized Fe grains. Recently, thermodynamically metastable structures have been generated during the electro-crystallisation process and this has given rise to a new and novel range of amorphous based Sn–Fe electrodeposited alloys [14]. Nanocrystalline $FeSn_2$ prepared by chemical reduction in tetraethylene glycol [15] and by reduction in aqueous and ethanol solutions [16] was recently reported. More recently, micro- and nano-$FeSn_2$ were compared by different researchers [17,18]. On the other hand, $Sn_{30}(Co_{1-x}Fe_x)_{30}C_{40}$ materials were prepared by Ferguson et al. [19] using mechanical attrition of $FeSn_2$, $CoSn_2$ and C, and amorphous grains of $Fe_xCo_{1-x}Sn$ in a carbon matrix were found. These authors found that the cobalt-free sample ($x = 1$) exhibits poor capacity retention on cycling.

In this work the formation of nanocrystalline particles composed of $Fe_{1-x}Co_xSn_2$ solid solutions by using a one-pot method is reported. For this purpose, the reduction of salts in an organic solvent below 200 °C is used. The tin nanocrystals are used as a template for the formation of intermetallic particles. Previous studies showed that the transition metals atoms can diffuse into β-Sn nanoparticles to form intermetallic phases [20].

2. Experimental

Powders of $Fe_{1-x}Co_xSn_2$ were obtained by following a tetraethylene glycol (TEG) method based on previous works [15,20]. For this purpose, $SnCl_2$, $FeCl_3{\cdot}6H_2O$ and $CoCl_2{\cdot}6H_2O$ were dissolved in TEG. All the samples were prepared under the same experimental conditions, except the variable ratio between the reagents cobalt chloride and iron chloride in order to modify the *x*-value in the nominal composition.

* Corresponding author. Tel.: +34 957218637; fax: +34 957218621.
E-mail address: iq1ticoj@uco.es (J.L. Tirado).

0925-8388/$ – see front matter © 2010 Elsevier B.V. All rights reserved.
doi:10.1016/j.jallcom.2010.11.202

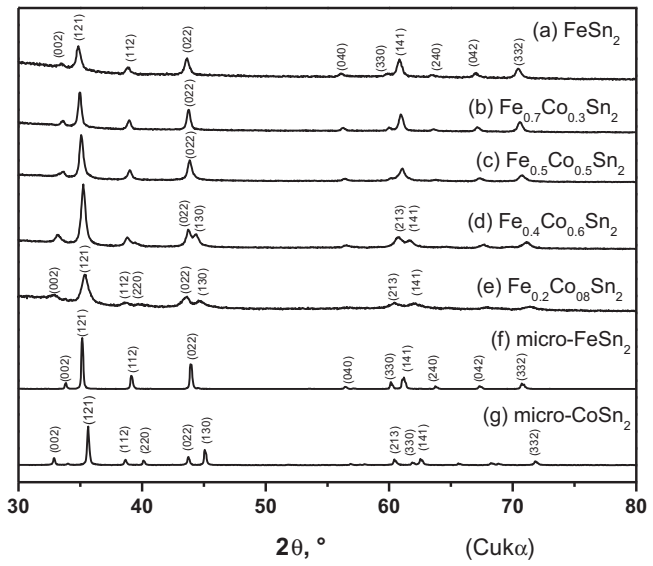

Fig. 1. XRD patterns of nanometric $Fe_{1-x}Co_xSn_2$ with $x = 0.0$, 0.25, 0.3, 0.5, 0.6 and 0.8. For the sake of comparison, the patterns for micrometric $FeSn_2$ and $CoSn_2$ are also shown in (f) and (g). The Miller indexes of the relevant reflections are indicated.

Poly(vinyl pyrrolidone) (PVP) and poly(2-ethyl-2-oxazoline) (PEO) were also added to the TEG. The polymers PEO and PVP are used to help the formation of very small metallic particles. $NaBH_4$ dissolved in TEG was used to reduce the ions. Firstly, the tin ions were reduced by adding the borohydride solution to the solution containing tin ions and polymers. Then, after stirring for 15 min at 170 °C, iron and cobalt ions solutions were sequentially added. The solution was then heated to 186 °C with continued stirring. The preparation was carried out under flowing argon to avoid the oxidation of the ions. The resulting powders were separated from the solvent by centrifugation, washed with ethanol and dried under vacuum at 80 °C.

Microcrystalline $CoSn_2$ and $FeSn_2$ were prepared by heating a mixture of the corresponding elements in the appropriate stoichiometric amounts under an argon atmosphere at 490 °C.

The Co/Fe relative content was obtained by element analysis carried out in a SEM instrument equipped with an EDAX detector. Particle morphology and structure were characterized by transmission electron microscopy (TEM) in a JEM2010 instrument and X-ray diffraction (XRD) in a Siemens D5000 instrument and using Cu Kα radiation. The lattice cell parameters were calculated by using the CELREF3 program. The ^{57}Fe Mössbauer spectra were obtained by using a WissEl instrument.

The electrochemical experiments were carried out in an Arbin system. For this purpose, lithium test cells were assembled in Ar-filled glove-box. A piece of lithium was used as the negative electrode. The positive electrode consisted of the intermetallic compound active material (77%), PVDF binder (8%) and carbon conductive agent (15%). The typical mass loading was 3 mg/cm^2. A solution of $LiPF_6$ in EC:DEC was used like electrolyte. The discharge–charge cycling experiments were conducted by imposing a determined current intensity and this current was mass-normalized.

3. Results and discussion

The XRD patterns of the obtained $Fe_{1-x}Co_xSn_2$ samples are shown in Fig. 1. Crystalline impurities were not observed. For $x \leq 0.5$, the patterns are close to the XRD ICDD file number 25-415 corresponding to $FeSn_2$ and could be indexed with tetragonal axis and in the space group $I4/mcm$ (number 140). Pure nanocrystalline $CoSn_2$ could not be prepared under the selected experimental conditions. When $x = 1$ was used as the starting composition, the resulting compound was $CoSn_3$. Due to the broadening of the Bragg peaks observed for the nanometric particles and for comparison, the XRD patterns of micrometric $CoSn_2$ and $FeSn_2$ prepared at 490 °C are shown in Fig. 1f and g. Irrespective of the isomorphic character, the XRD patterns of $CoSn_2$ and $FeSn_2$ show certain differences, as a consequence of their different unit cell parameters. According to the ICDD file number 25-256, two Bragg peaks are observed between 43 and 46° 2θ for pure $CoSn_2$, which correspond to (0 2 2) and (1 3 0) reflections, while only one peak is resolved in this range for $FeSn_2$ (ICDD file number 25-415). In addition, the (2 2 0) reflection is observed for $CoSn_2$ at 40.1° 2θ, but it is not detected for $FeSn_2$, and this result is also in good agreement with the XRD files numbers 25-415 and 25-256. The obtained nanometric $Fe_{1-x}Co_xSn_2$ samples show XRD patterns intermediate between $CoSn_2$ and $FeSn_2$. The refinement by using the peaks positions leads to the lattice cell parameters that are shown in Fig. 2a. For the sake of comparison the data from ICDD files are also included in Fig. 2. For $FeSn_2$ (ICDD file number 25-415), $a = 6.539$ and $c = 5.325$ Å. For $CoSn_2$ (ICDD file number 25-256), $a = 6.363$ and $c = 5.456$ Å. Hence, the influence of stoichiometry (x-value) on the unit cell parameters is complicated by the feature that $a(FeSn_2) > a(CoSn_2)$ but $c(FeSn_2) < c(CoSn_2)$. The atomic radius of Co (125 pm) is slightly smaller than the corresponding radius of Fe (126 pm) [21] and a small linear decrease of the unit cell volume is expected according to the Vegard's law. Such behaviour is experimentally observed when cobalt content increases in nano-$Fe_{1-x}Co_xSn_2$ solid solutions (Fig. 2b). The lattice parameter a decreases on increasing cobalt content while the observed evolution of the c unit cell parameter is more complex. Below $x = 0.5$ the c parameter slightly decreases with cobalt content and from $x > 0.5$ to $x = 0.8$ increases. The deviations of the Vegard's law are usual [22].

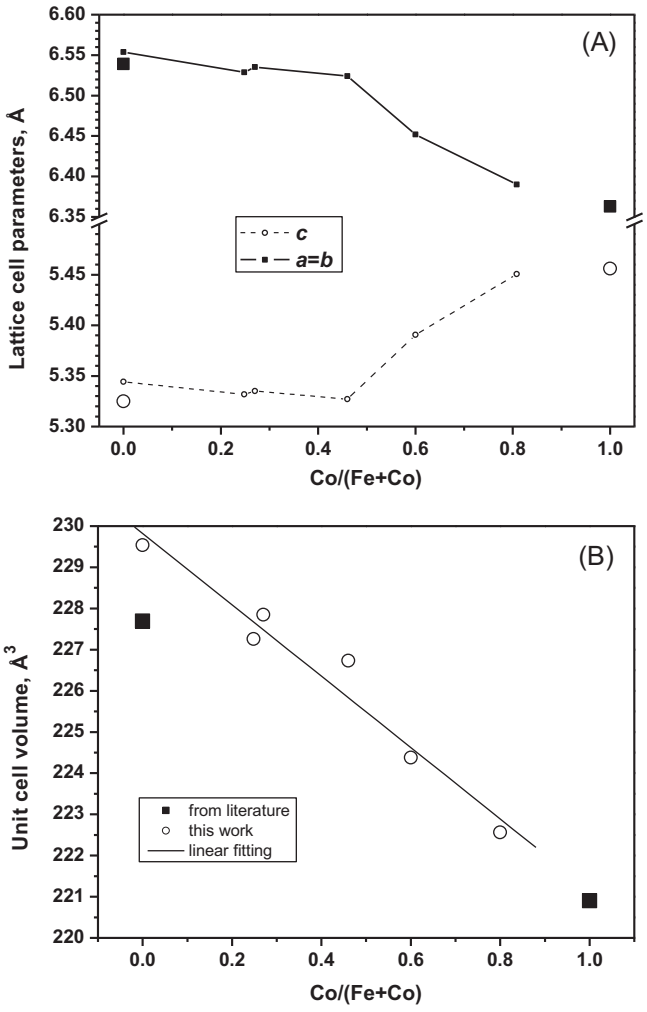

Fig. 2. (a) Evolution of the tetragonal lattice cell parameters as a function of cobalt content in nanocrystalline $Fe_{1-x}Co_xSn_2$. The parameters taken from the literature for pure $FeSn_2$ (XRD file no. 25-415) and $CoSn_2$ (XRD file no. 25-256) are also shown like bigger points. (b) Volume of the unit cell and linear fitting of the obtained experimental data. The volume cell values taken from the literature are represented by the symbol (■).

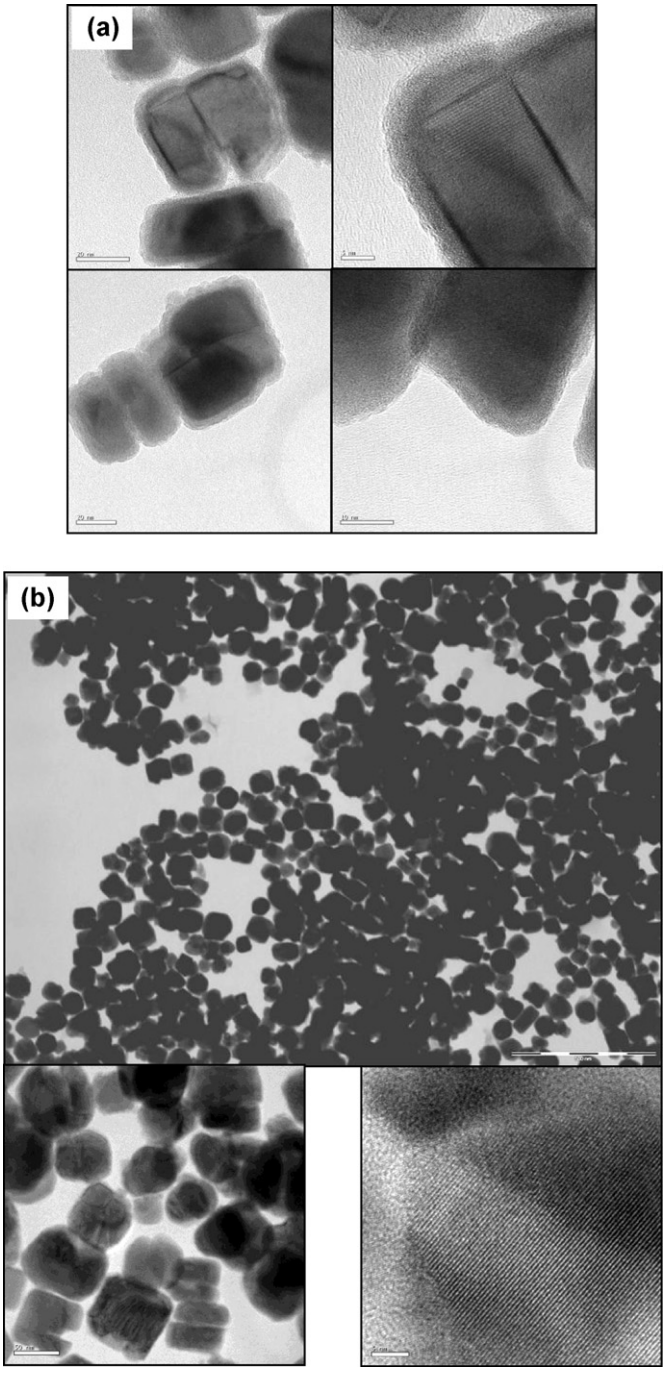

Fig. 3. Selected TEM images for (a) $Fe_{0.8}Co_{0.2}Sn_2$ and (b) $Fe_{0.5}Co_{0.5}Sn_2$.

Selected TEM images of $Fe_{1-x}Co_xSn_2$ are shown in Fig. 3. Particle size is in the order of 20 nm. Lattice fringes are observed evidencing the nanocrystalline nature of the samples. The observed nanocrystals have morphologies of cubes, rounded-cubes, U-shaped and nanorod dimers. A poorly crystalline shell surrounds the intermetallic particles that may be ascribed tentatively to an XRD-undetected SnO_x layer. All these observations are consistent with the previous studies on nanocrystalline $FeSn_2$, where a mechanism based on the Kirkendall effects was proposed for the formation of the nanoparticles [20]. The cubic particles of β-Sn are formed first and serve as seeds for the growth of intermetallic particles. Iron and cobalt formed under reducing conditions diffuse into the tin particles. The different diffusion rates of Sn, Co and Fe atoms can cause the occurrence of voids in the intermetallic particles and

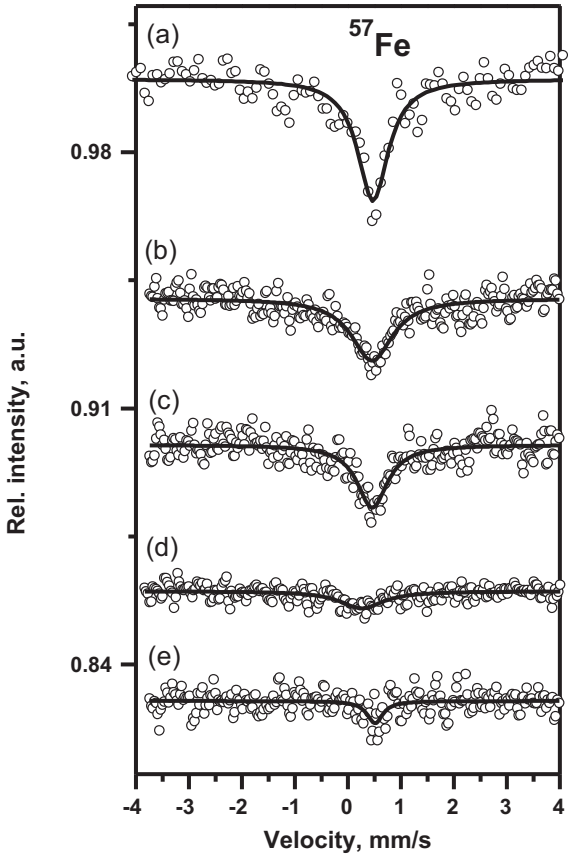

Fig. 4. Room temperature ^{57}Fe Mössbauer spectra for nanocrystalline $Fe_{1-x}Co_xSn_2$ with x equals to 0.0 (a), 0.25 (b), 0.3 (c), 0.5 (d) and 0.8 (e).

the formation of nanorods, particularly in the case of β-Sn seeds larger than 30 nm. The smaller cube shaped β-Sn (<15 nm) seeds transform to dense intermetallic particles (not hollow) preserving their cubic form [20].

The nanometric character and the composition of the nano-$Fe_{1-x}Co_xSn_2$ samples influence the ^{57}Fe Mössbauer spectra. Thus, the hyperfine magnetic fields are not present, in contrast to microcrystalline $FeSn_2$ [23], indicating the superparamagnetic character of the studied samples. Irrespective of the low intensity for the samples with low iron-content, the room temperature ^{57}Fe Mössbauer spectra (Fig. 4) of all the nanosized $Fe_{1-x}Co_xSn_2$ samples are rather similar and can be ascribed to a superparamagnetic singlet, as was previously described for nano-$FeSn_2$ [14,24]. In contrast, microcrystalline $FeSn_2$ shows a sextuplet signal at room temperature due to long-range magnetism [13,25]. In $FeSn_2$, each iron atom is in a high symmetry site and is surrounded by eight tin atoms at the corners of a square antiprism. Trumpy et al. found that in the iron–tin system, the electron densities are reduced at all the nuclei with respect to the pure metals, and the isomer shifts were linearly related to the number of Fe–Sn bonds in such a way that bonding reduces the electron densities at both nuclei [23]. The distances between the atoms in the alloys also can contribute to the change of the isomer shift. The ^{57}Fe isomer shift tends to decrease when the iron content decreases and the cobalt content increases (Fig. 5). This result indicates that the electron density between Fe and Sn increases when the amount of cobalt increases, suggesting that the Fe–Sn bond becomes stronger, in good agreement with the observed decrease of the lattice cell parameters. The sample with $x = 0.8$ shows certain deviation from the general tendency, but it is within the experimental error due to the lower iron content and poorer crystallinity of this sample. The low crystallinity can

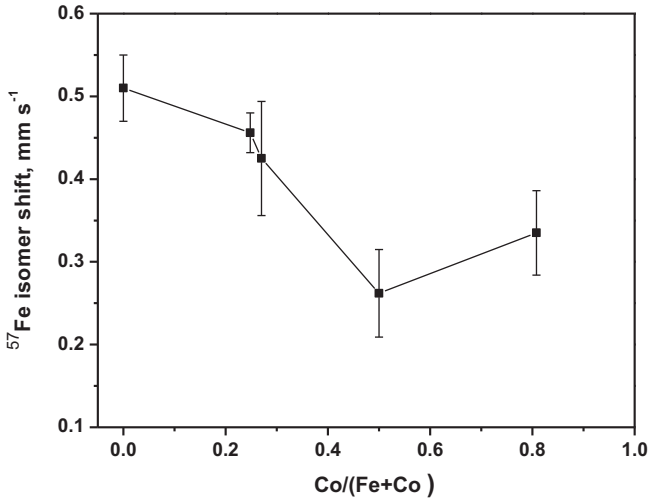

Fig. 5. ^{57}Fe isomer shift as a function of cobalt content.

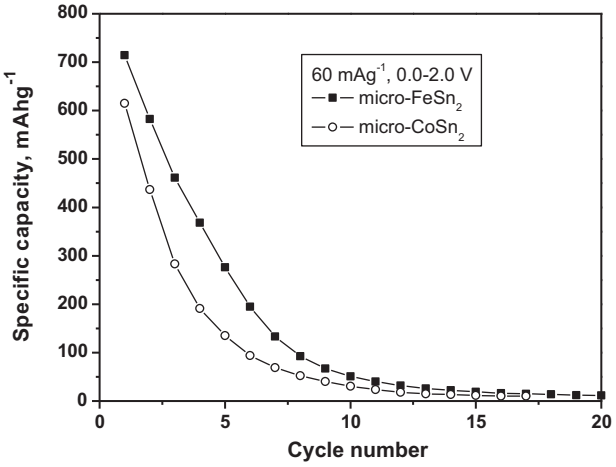

Fig. 6. Specific capacity as a function of cycle number for microcrystalline $FeSn_2$ and $CoSn_2$ in lithium test cells.

decrease the Lamb-Mössbauer factor and can result in some uncertain. Otherwise, the increase of the c-lattice cell parameter from $x = 0.5$ to $x = 0.8$ may be related to the relative increase of the ^{57}Fe isomer shift.

The electrochemical behaviour of nano-$Fe_{1-x}Co_xSn_2$ was studied in lithium test cells. For the sake of comparison, the capacity retention of microcrystalline $CoSn_2$ and $FeSn_2$ materials are shown in Fig. 6, and very poor capacity retention is observed in both cases. It has been reported that isostructural $FeSn_2$ and $CoSn_2$ have tunnels between the Sn atoms in their structure, where Li can penetrate to initiate the reaction and form Li_xSn alloys, but the facility for lithium intercalation is dependent on particle size [26]. Due to the insertion and extraction of lithium, the large particles of alloy can suffer abrupt volume changes, swelling and break-up, yielding to the occurrence of electrically disconnected particles and battery failure. Irrespective of the fact that the capacity retention of all the samples are significantly influenced by the experimental condition, the best electrochemical behaviour of the nano-$Fe_{1-x}Co_xSn_2$ samples (Fig. 7) is much better than the corresponding micro-$CoSn_2$ and micro-$FeSn_2$ (Fig. 6). The best

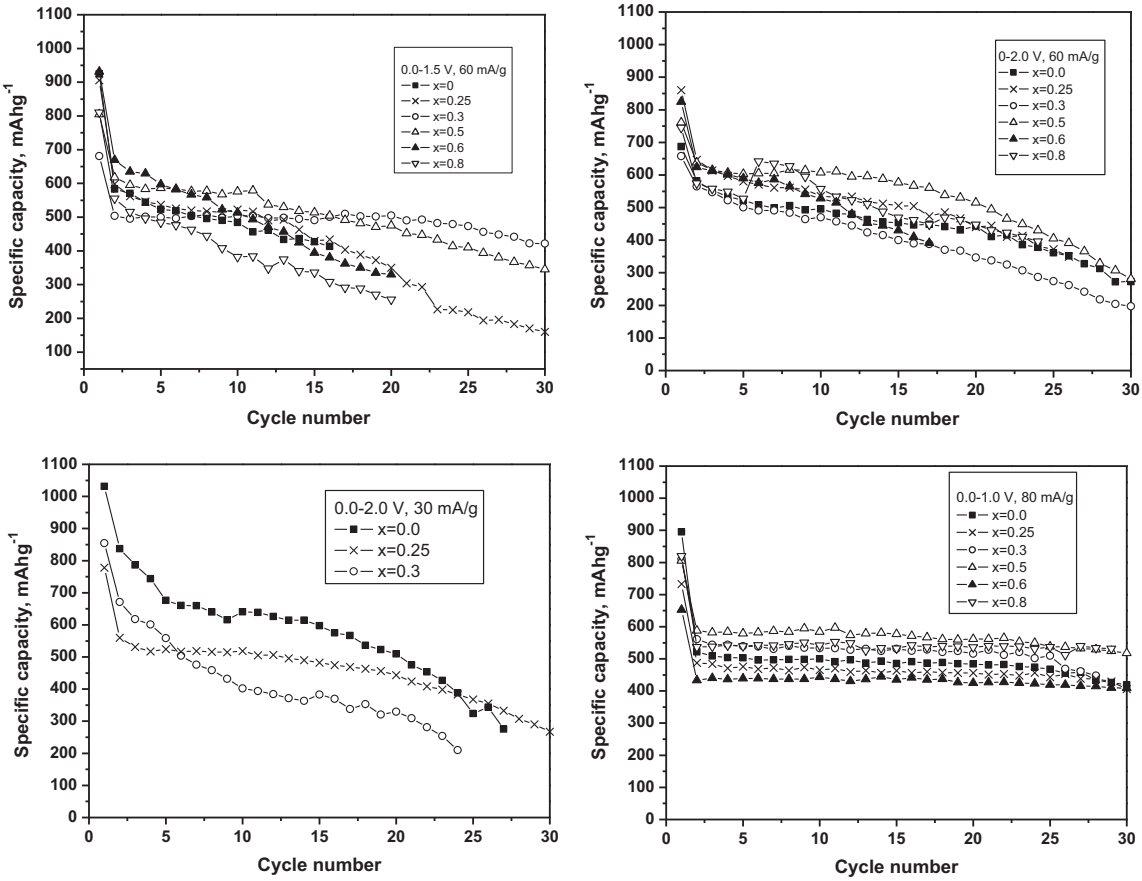

Fig. 7. Specific capacity as a function of cycle number for $Fe_{1-x}Co_xSn_2$ in lithium test cells under several experimental conditions.

electrochemical behaviour is observed for $x = 0.5$, with maximum capacities values above 500 mAh g^{-1} after 30 cycles. More probably, the simultaneous presence of two transition metals and the nanometric character improves the metallic glass-forming ability, avoids the crystal growth and improves the cycling stability. Several current intensities and potential windows have been tested. At 60 mA g^{-1} of mass-normalized current intensity, the capacity retention is improved when the upper potential limit is decreased from 2.0 to 1.5 V. The initial capacity is higher at 30 mA g^{-1} than at 60 mA g^{-1} (in the 0.0–2.0 potential window), but the capacity fades more rapidly at 30 mA g^{-1}. In conclusion, capacity retention improves when the upper potential limit is decreased from 2.0 to 1.0 and the current intensity is increased from 30 to 80 mA g^{-1}. Most probably, the higher current intensities decrease the extension of irreversible processes and lead to better cycling stability.

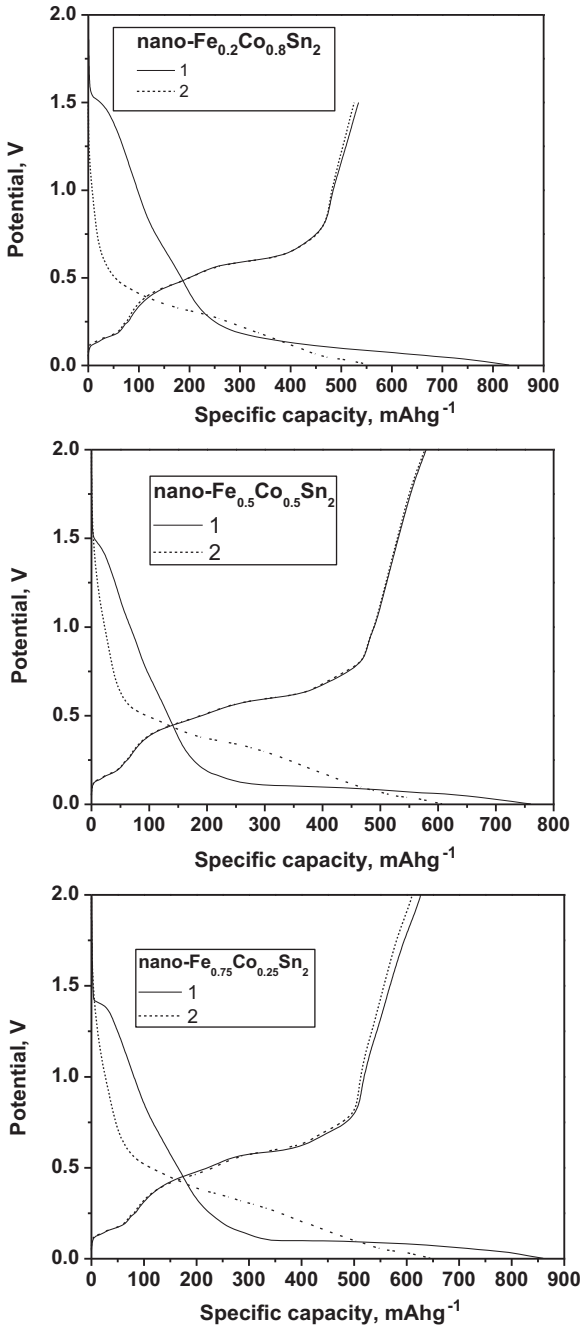

Fig. 8. Potential–capacity plots of selected samples.

The electrochemical behaviour of nano-$Fe_{1-x}Co_xSn_2$ could be further improved by using a carbonaceous matrix and by optimization of the binding agent.

The potential–capacity curves corresponding the first and second discharge–charge cycle of representative nanometric samples are shown in Fig. 8. All the nano-$Fe_{1-x}Co_xSn_2$ samples have rather similar discharge–charge profile. These nanometric samples and the micrometric $CoSn_2$ [4,26] and $FeSn_2$ [15] samples do not differ greatly in their potential–capacity profiles. However, the surface reactions would be more extensive for very small particles. The reaction between lithium and the amorphous oxide layer through conversion reaction and formation of a solid electrolyte interphase (SEI) [26] can contribute to the irreversible capacity of the first cycle and to decrease the coulombic efficiency. The irreversible formation of Li_2O and SEI would be more extended for the very small particles. Thus, the efficiency for the first cycle of nano-$Fe_{0.5}Co_{0.5}Sn_2$ in Fig. 8 is 76%, and the efficiency observed for micro-$FeSn_2$ and micro-$CoSn_2$ is 82 and 79%, respectively. Zhang and Xia previously reported a coulomb efficiency of 85% for microcrystalline $CoSn_2$ [26]. The higher reactivity of the surface (SEI formation) for nano-$FeSn_2$ in comparison with micro-$FeSn_2$ has been recently reported elsewhere [18]. On the other hand, the formation of a Li_2O matrix after the reaction between surface oxide and lithium may contribute to buffer the volume change during the processes of lithium insertion–extraction in the metallic particles, and to improve the capacity retention upon cycling of the nanoparticles. In addition, the destruction of the Li_2O matrix at the upper potential limit around 2 V may yield to strong capacity fade upon

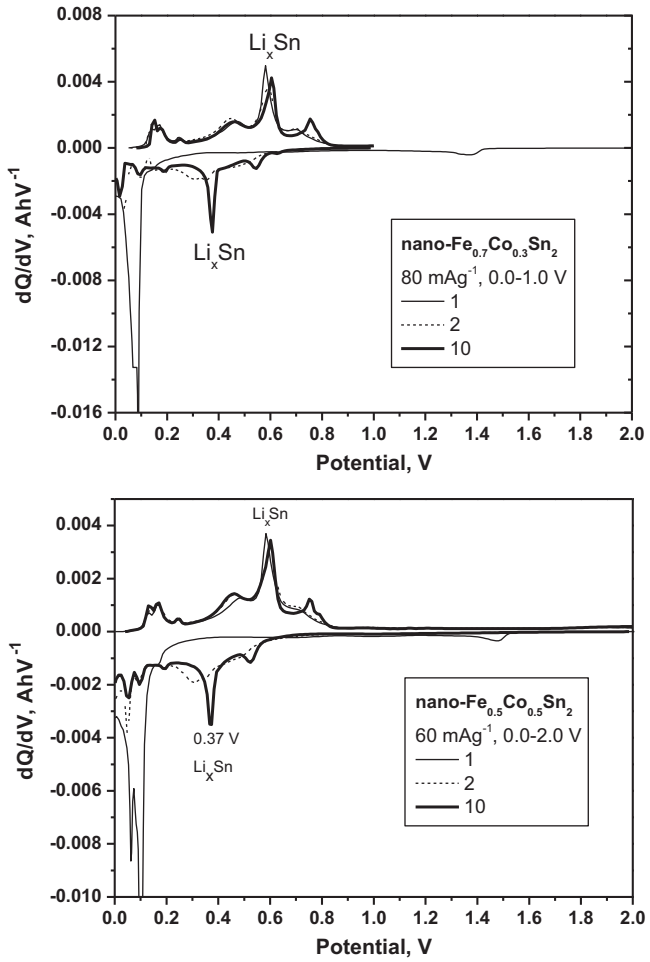

Fig. 9. Selected derivative curves.

cycling (Fig. 7). The main problem of the initial irreversible capacity would be the consumption of lithium from the positive electrode in a lithium ion battery.

The derivative plots (dQ/dV vs. potential) for $x = 0.3$ and $x = 0.5$ are shown in Fig. 9 and can be used to explore the electrochemical reactions. An irreversible peak at around 1.4 V is observed in the first discharge process that can be ascribed to formation of passivating surface film (SEI). The main reaction of the first discharge is observed as a very intense peak located below 0.2 V. After the first cycle, the derivative curves remain almost without change, suggesting a good stability of the electrode active material. The occurrence of Li_xSn alloys is observed as a peak at ca. 0.38 V in the successive discharges and several peaks at 0.45, 0.6 and 0.75 V in the charge processes. The $Fe_{1-x}Co_xSn_2$ samples with both iron and cobalt in their composition, as well as $FeSn_2$ [18], exhibit peaks in the first charge (0.6 V) and second discharge (0.4 V) that are ascribed to formation of Li_xSn phases. In contrast, the cobalt–tin phases CoSn [2], $CoSn_2$ [3,4] and $CoSn_3$ [9] do not show these narrow peaks. Hence, the iron–cobalt sample forms Li–Co–Sn alloys or form very small grains of Li–Sn alloys that interact with Co atoms. However, the iron-containing samples have greater tendency to form crystalline grains of Li_xSn phases. It is noteworthy that cobalt and tin have strong tendency to form amorphous alloys [27,28]. It seems that the simultaneous presence of two transition metals ($x = 0.5$), one of them (Co) with greater ability to alloy with Sn and another (Fe) with lower ability to alloy with Sn, favours a better electrode stability.

4. Conclusions

The electrochemical behaviour of the intermediate nano-$Fe_{1-x}Co_xSn_2$ compositions is better than the corresponding micro-$CoSn_2$ and $FeSn_2$. Particularly promising is the electrochemical behaviour for intermediate compositions ($x = 0.5$). The TEG-method can be used at relatively low temperatures (around 200 °C) to obtain intermetallic compounds, but other preparation methods, more adequate for an industrial scale, should be developed. The incorporation of cobalt in the framework leads to a decrease of the volume of the unit cell and the Mössbauer hyperfine parameters are modified. The samples that contain iron form Li_xSn phases during the discharge of the cell and exhibit capacities over 500 mAh g^{-1} during the first 30 cycles and within the potential window between 0.0 and 1.0 V.

Acknowledgements

R.A. acknowledges the financial support from MICNN (CTQ2008-03192). U.G.N. thanks to Alistore-ERI for a grant. J.L.T. acknowledges the financial support from MICINN (MAT2008-05880). Electron microscopy was performed at the SCAI at Córdoba University.

References

[1] P.P. Ferguson, M.L. Martine, A.E. George, J.R. Dahn, J. Power Sources 194 (2009) 794.
[2] R. Alcántara, I. Rodríguez, J.L. Tirado, Chem. Phys. Chem. 9 (2008) 1171.
[3] C.M. Ionica-Bousquet, P.E. Lippens, L. Aldon, J. Olivier-Fourcada, J.C. Jumas, Chem. Mater. 18 (2006) 6442.
[4] R. Alcántara, G. Ortiz, I. Rodríguez, J.L. Tirado, J. Power Sources 189 (2009) 309.
[5] J.S. Thorne, P.P. Ferguson, R.A. Dunlap, J.R. Dahn, J. Alloys Compd. 472 (2009) 390.
[6] J. Li, D.B. Le, P.P. Ferguson, J.R. Dahn, Electrochim. Acta 55 (2010) 2991.
[7] F. Nacimiento, R. Alcántara, J.L. Tirado, J. Alloys Compd. 485 (2009) 385.
[8] F. Nacimiento, R. Alcántara, J.L. Tirado, J. Power Sources, in press, doi:10.1016/j.jpowsour.2010.11.034.
[9] R. Alcántara, U. Nwokeke, I. Rodríguez, J.L. Tirado, Electrochem. Solid State Lett. 11 (2008) A209.
[10] J. Xie, X.B. Zhao, G.S. Cao, J.P. Tu, J. Power Sources 164 (2007) 386.
[11] J.R. Dahn, R.E. Mar, A. Abouzeid, J. Electrochem. Soc. 153 (2006) A361.
[12] J. He, H. Zhao, J. Wang, J. Wang, J. Chen, J. Alloys Compd. 508 (2010) 629.
[13] O. Mao, R.D. Dunlap, J.R. Dahn, J. Electrochem. Soc. 146 (1999) 405.
[14] C.U. Chisholm, E. El-Sharif, S. Kuzmann, Z. Stichleutner, A. Homonnay, Vertes, Mater. Chem. Phys. 120 (2010) 558.
[15] U.G. Nwokeke, R. Alcántara, J.L. Tirado, R. Stoyanova, M. Yoncheva, E. Zhecheva, Chem. Mater. 22 (2010) 2268.
[16] C.Q. Zhang, J.P. Tu, X.H. Huang, Y.F. Yuan, S.F. Wang, F. Mao, J. Alloys Compd. 457 (2008) 81.
[17] M. Chamas, P.E. Lippens, J.C. Jumas, K. Boukerma, R. Dedryvère, D. Gonbeau, J. Hassoun, S. Panero, B. Scrosati, J. Power Sources, in press, doi:10.1016/j.jpowsour.2010.09.113.
[18] U.G. Nwokeke, R. Alcántara, J.L. Tirado, R. Stoyanova, E. Zhecheva, J. Power Sources, in press, doi:10.1016/j.jpowsour.2010.10.071.
[19] P.P. Ferguson, P. Liao, R.A. Dunlap, J.R. Dahn, J. Electrochem. Soc. 156 (2009) A13.
[20] N.H. Chou, R.E. Schaak, J. Am. Chem. Soc. 129 (2007) 7339.
[21] N.N. Greenwood, A. Earnshaw, Chemistry of the Elements, Butterworth-Heinemann, 1998.
[22] K.T. Jacob, S. Raj, L. Rannesh, Int. J. Mater. Res. (2007) 776.
[23] G. Trumpy, E. Both, C. Djéga-Mariadassou, P. Lecocq, Phys. Rev. B 2 (1970) 3477.
[24] R.A. Dunlap, O. Mao, J.R. Dahn, Phys. Rev. B 59 (1999) 3494.
[25] B. Wodniecka, P. Wodniecki, A. Kulinska, A.Z. Hrynkiewicz, J. Alloys Compd. 321 (2001) 1.
[26] J.J. Zhang, Y.Y. Xia, J. Electrochem. Soc. 153 (2006) A1466.
[27] N. Tamura, M. Fujimoto, M. Kamino, S. Fujitani, Electrochim. Acta 49 (2004) 1949.
[28] P. Guilmin, P. Guyot, G. Marchal, Phys. Lett. 109 (1985) 174.